Available online at www.sciencedirect.com
SCIENCE DIRECT®
Journal of Colloid and Interface Science 271 (2004) 110–119
JOURNAL OF Colloid and Interface Science
www.elsevier.com/locate/jcis

Aggregate formation and collision efficiency in differential settling

Albert S. Kim [a,*] and Keith D. Stolzenbach [b]

[a] *Department of Civil and Environmental Engineering, University of Hawaii at Manoa, Honolulu, HI 96822, USA*
[b] *Department of Civil and Environmental Engineering, University of California, Los Angeles, CA 90095-1593, USA*

Received 10 October 2002; accepted 8 October 2003

Abstract

A new method of application of Stokesian dynamics, which can efficiently simulate movements of up to 500 particles with interparticle interactions in reasonable computational times, has been developed for the purpose of investigating particle–cluster aggregation in aqueous systems. The method is applied to monodisperse non-Brownian spherical particles aggregating in differential settling, while repulsive colloidal interaction is presumed to be negligible, so that a minimum separation distance can represent the attractive van der Waals force. The final aggregates formed by this algorithm, composed of 300 primary particles, have a common fractal dimension of ∼2.0. The computed collision efficiency, defined as the product of a global and a capture efficiency, is about 5.77×10^{-3}. This value is significantly larger than the collision efficiency of primary particles colliding with an impermeable solid sphere of the same size as the aggregate, illustrating the important interplay between the permeability and the formation of aggregates.

Keywords: Aggregate formation; Aggregate permeability; Fractal structure; Efficiency; Differential settling; Stokesian dynamics simulation

1. Introduction

In natural waters as well as water and wastewater treatment systems, large porous aggregates are formed by collisions among suspended particles and/or relatively small aggregates. The aggregation of particles in the aqueous systems occurs by Brownian motion [1], turbulent shear flow [2], or differential settling [3]. For example, in natural (i.e., ocean) water bodies, aggregates composed of living cells are formed by turbulent shear in near-surface layers and rapidly settle to the sea floor, transporting material from surface layers to sediments. On the other hand, in conventional water and wastewater treatment systems, microbial aggregates are removed within clarifiers by differential settling. In these cases, when flow penetrates into a permeable aggregate, some small particles in the internal flow will be able to collide with and attach to the aggregate, so that the capture of the small particles by the aggregate is highly dependent on aggregate structure, which can be represented by a fractal dimension. Therefore, generation of a realistic aggregate by computer simulation is important to the investigation of the structure and the role of aggregates created in engineered and natural water systems.

Once a large aggregate, composed of many primary particles, is formed by a certain mechanism (including differential settling), differential settling plays an important role in particle–cluster aggregation due to the much faster sinking velocity of the aggregate than of (suspended) primary particles. In addition to density and solid volume fraction, the aggregate structure, characterized by the fractal dimension, is known to have significant affects on the aggregate sinking velocity. For particle capture, Han and Lawler calculated collision efficiency between two rigid spherical particles using trajectory analysis [4]; Wacholder and Sather [5] have investigated the influence of size and density on efficiency; and the effect of the van der Waals force for this case has been considered by Mazzolani et al. [6]. None of these studies, however, dealt with effect of fractal–aggregate permeability, which results in flow penetrating the aggregates, potentially increasing the capture of primary particles in comparison to an impermeable sphere.

In this work, Stokesian dynamics (SD), a molecular-dynamics-like approach developed by Brady and Bossis [7], is used, with a computationally effective algorithm, to generate aggregates in differential settling and to investigate structure of the aggregate, and this methodology is then applied to

* Corresponding author.
E-mail address: albertsk@hawaii.edu (A.S. Kim).

0021-9797/$ – see front matter
doi:10.1016/j.jcis.2003.10.014

compute the collision efficiency of suspended primary particles by the porous sinking aggregate.

2. Simulation method

2.1. Particle–cluster aggregation in differential settling: Stokesian dynamics simulation

In differential settling, for example, sedimentation tanks or deep marine systems, the components of the ambient velocity, i.e., the constant unidirectional flow $\mathbf{U}^\infty$, the vorticity $\boldsymbol{\Omega}^\infty$, and the strain rate $\mathbf{E}^\infty$, are usually all negligible, so that the translational and rotational velocities of all particles are mainly affected by applied forces and torques. In particle–cluster aggregation, a sinking aggregate composed of N_a identical primary particles interacts hydrodynamically with (suspended) individual primary particles of the same size, consequently resulting in the two-body problem at dilute particle concentrations. These lead to two important assumptions in applying the SD to the aggregation phenomena, specifically in the differential settling. First, each particle associated with the aggregate translates at the same sinking velocity without individual rotation relative to other particles. Second, the lubrication interaction is important only between the suspended primary particle and each of the N_a aggregated particles, because the (moving) suspended particle does not have any geometrical constraint to the aggregate, and its rotation is not prevented. Furthermore, it is worth noting that, even though pairwise lubrication interaction [8,9] can be added onto the inverse grand mobility matrix $(\mathcal{M}^\infty)^{-1}$ in a consistent manner [10], it does lead to significant overestimation in evaluating hydrodynamic interactions among N_a particles geometrically stuck to each other [11]. Therefore, in the absence of the imposed shear flow the F–T version of the SD is appropriate when considering only the uniform translation of the aggregate and the translation/rotation of the single suspended particle for which the lubrication force is not negligible in near contact to any of the N_a aggregated particles [10]. On the other hand, it is also possible to mix two versions of Stokesian dynamics, i.e., the F version for the aggregate and F–T version for the single particle, according to the components of its movement. Although the computation effort may be several times less, this mixed version approach probably reduces the simulation accuracy compared to the full F–T version, especially when the single particle is very close to some of the fixed particles within the aggregate. In the F–T version, the size of the grand mobility matrix $\mathcal{M}^\infty$ for the N_a aggregated particles and one single moving particle is $6N \times 6N$, divided into $3N$ for forces and another $3N$ for torques, where $N = N_a + 1$. The CPU time for the F–T version of the SD simulation is quite expensive because of the need to invert the large grand mobility matrix $\mathcal{M}^\infty$. However, computationally effective partitioning methods are available somewhere else for application to particle–cluster aggregation [12,13].

For the N_a nonrotating aggregated particles in the absence of external torques and ambient flow, the grand resistance matrix can be reduced and rewritten in an expanded form with respect to the particle index,

$$\begin{bmatrix} \mathbf{F}_1 - \boldsymbol{\psi}_1 \\ \vdots \\ \mathbf{F}_{N_a} - \boldsymbol{\psi}_{N_a} \\ \mathbf{F}_s \\ 0 \end{bmatrix} = \begin{bmatrix} R_{U_1}^{F_1} & \cdots & R_{U_{N_a}}^{F_1} & \mathbf{R}_{U_s}^{F_1} & \mathbf{R}_{\Omega_s}^{F_1} \\ \vdots & \ddots & \vdots & \vdots & \vdots \\ R_{U_1}^{F_{N_a}} & \cdots & R_{U_{N_a}}^{F_{N_a}} & \mathbf{R}_{U_s}^{F_{N_a}} & \mathbf{R}_{\Omega_s}^{F_{N_a}} \\ \mathbf{R}_{U_1}^{F_s} & \cdots & \mathbf{R}_{U_{N_a}}^{F_s} & \mathbf{R}_{U_s}^{F_s} & \mathbf{R}_{\Omega_s}^{F_s} \\ \mathbf{R}_{U_1}^{T_s} & \cdots & \mathbf{R}_{U_{N_a}}^{T_s} & \mathbf{R}_{U_s}^{T_s} & \mathbf{R}_{\Omega_s}^{T_s} \end{bmatrix} \cdot \begin{bmatrix} \mathbf{U}_a \\ \vdots \\ \mathbf{U}_a \\ \mathbf{U}_s \\ \boldsymbol{\Omega}_s \end{bmatrix}, \tag{1}$$

where F_i (for $i = 1, \ldots, N_a$) is the force exerted on each of the aggregated particles; ψ_i is the constraint force that keeps unchanged the distances from the ith particle to the rest of the $N_a - 1$ particles within the aggregate; U_a is the common unidirectional velocity of all the N_a aggregated particles, i.e., $\mathbf{U}_1 = \cdots = \mathbf{U}_N = \mathbf{U}_a$; and U_s, Ω_s, and F_s are the translational and rotational velocity of and the force exerted on the single particle, respectively. The size of the reduced grand resistance matrix in Eq. (1) is $(3N_a + 6) \times (3N_a + 6)$, representing $3N_a$ components of forces acting on the N_a aggregated particles and 6 components of both force and torque on the single particle (note that the far-field part of this matrix is different from the inverted form of the mixed $(3N_a + 6) \times (3N_a + 6)$ grand mobility matrix with only the F version for the aggregate and the F–T version for the single particle). Because any two particles within the aggregate have zero relative rotational and translational velocity, the pairwise lubrication term is not included in the many-body interactions of $R_{U_i}^{F_i}$, $R_{\Omega_i}^{F_i}$, $R_{U_i}^{T_i}$, and $R_{\Omega_i}^{T_i}$ for $i = 1, \ldots, N_a$, as denoted by italic characters in Eq. (1). However, the hydrodynamic interactions between the single particle and the N_a aggregated particles, as written by bold characters in Eq. (1), has been updated by addition of the lubrication interaction if and only if the gap (surface-to-surface distance between two primary particles) is less than the diameter of the primary particle. Each submatrix R_j^i (or $\mathbf{R}_j^i$) represents the coupling of the forces or torques and translational or rotational velocities with (or without) the lubrication interaction.

The forces exerted on each of the $N_a + 1$ particles in differential settling are obviously gravity and buoyancy, which are external forces that are independent of interparticle distances; i.e.,

$$\mathbf{F}_i = \mathbf{F}_{\text{ext}} = \frac{4\pi}{3} a^3 (\rho_p - \rho_f) g, \tag{2}$$

where ρ_p and ρ_f are the densities of the primary particle and the fluid, respectively, a is the radius of the particle, and

g is the gravitational acceleration. Thus, the $(3N_a + 6) \times (3N_a + 6)$ grand resistance matrix of Eq. (1) can be significantly reduced to the 9×9 matrix

$$\begin{bmatrix} N\mathbf{F}_{\text{ext}} \\ \mathbf{F}_{\text{ext}} \\ 0 \end{bmatrix} = \begin{bmatrix} \sum_{i,j}^{N_a} R_{U_j}^{F_i} & \sum_{i}^{N_a} \mathbf{R}_{U_s}^{F_i} & \sum_{i}^{N_a} \mathbf{R}_{\Omega_s}^{F_i} \\ \sum_{i}^{N_a} \mathbf{R}_{U_i}^{F_s} & \mathbf{R}_{U_s}^{F_s} & \mathbf{R}_{\Omega_s}^{F_s} \\ \sum_{i}^{N_a} \mathbf{R}_{U_i}^{T_s} & \mathbf{R}_{U_s}^{T_s} & \mathbf{R}_{\Omega_s}^{T_s} \end{bmatrix} \begin{bmatrix} \mathbf{U}_a \\ \mathbf{U}_s \\ \boldsymbol{\Omega}_s \end{bmatrix}, \tag{3}$$

where

$$\sum_{i}^{N_a} \boldsymbol{\psi}_i = 0, \tag{4}$$

so that the sum of the "internal" force $\boldsymbol{\psi}_i$ vanishes, mechanically constraining the relative geometry of the N_a aggregated particles. Equation (3) therefore governs the movement of the single particle with the rotational velocity $\boldsymbol{\Omega}_s$, approaching the aggregate with the relative translational velocity

$$\mathbf{U}_{\text{rel}} = \mathbf{U}_s - \mathbf{U}_a. \tag{5}$$

Thus, the first-order time evolution equation for the relative position $\mathbf{x}_s$ of the single particle to the center of mass of the aggregate is

$$\frac{d\mathbf{x}_s}{dt} = \mathbf{U}_{\text{rel}}, \tag{6}$$

the solution of which is obtained by the Runge–Kutta method [14]. The simulation procedure is described in following sections.

3. Aggregate formation

3.1. Simulation algorithm

In simulating aggregate formation, because of the greater size and mass of the aggregate relative to a single particle, it is assumed that the rotation of the whole aggregate, composed of N_a nonrotating primary particles stuck to each other, is not affected by the presence of the suspended primary particle, unlike the absolute sinking velocity of the aggregate, as described in Eq. (3).

For simplicity, the spatial origin at the center of mass position of the aggregate is selected because the downward approach of the aggregate toward the suspended primary particle is equivalent to the upward movement of the single particle to the aggregate in the relative coordinate system. The initial position of the primary particle is randomly selected below the aggregate at (x_{s0}, y_{s0}, z_{s0}), which is determined by the necessary conditions

$$\begin{aligned} &-z_{s0} < R_{\max} + a, \\ &\sqrt{x_{s0}^2 + y_{s0}^2} \leqslant R_{\max} + a, \end{aligned} \tag{7}$$

where $R_{\max}$ is the distance from the center of mass of the aggregate to the outer edge of the outermost primary particle associated with the aggregate. Usually, z_{s0} is selected sufficiently far from the aggregate so that the ratio of $|z_{s0}/(R_{\max} + a)|$ is greater than at least 2.0. After the suspended primary particle is created at the random position (x_{s0}, y_{s0}, z_{s0}), the next position is calculated by solving the time evolution equation (6) using the Runge–Kutta scheme.

When the primary particle approaches one of the N_a aggregated particles in the relative coordinate system such that the gap between two particles become less than a certain percentage of the radius a of the monodisperse primary particles, the single particle is considered to be captured by the aggregate, adding one to the total number of aggregated particles. The rationale for this minimum gap is discussed in the next section. It is worth noting that, for the low Reynolds number and dilute particle concentration conditions assumed here, the relative approach velocity of the primary particle does not affect the structure of the growing aggregate, but controls only the growth rate of aggregation.

If the primary particle is deflected away from the center of mass of the aggregate by repulsive hydrodynamic interaction, i.e.,

$$\sqrt{x_s^2 + y_s^2} > R_{\max} + a, \tag{8}$$

with an arbitrary value of z_s, or escapes the aggregate by penetrating into its central region, i.e.,

$$\begin{aligned} &z_s > R_{\max} + a, \\ &\sqrt{x_s^2 + y_s^2} \leqslant R_{\max} + a, \end{aligned} \tag{9}$$

where (x_s, y_s, z_s) is the position of the single particle at time t (> 0), then the calculation for that particle is terminated and another particle is released at a new random starting position (x_{s0}, y_{s0}, z_{s0}), satisfying Eq. (7).

After a single particle is captured by the mechanism described above, the whole aggregate is assumed to undergo a random rotation representing the orientation change of the aggregate resulting from local vorticity in a turbulent flow environment. A corollary assumption is that the length scale of the smallest turbulent motions is greater than the size of the aggregate. In addition, the level of turbulence is assumed to be sufficiently small that the resulting fluid shear does not significantly affect the sinking speed of the aggregate or the rate of collision of the aggregate with the primary particles. Similar assumptions about the randomizing effect of local turbulence on the orientation of a settling particle were made by Batchelor [15] for the case of diffusive mass transfer from settling particles. The superposition of low-level turbulence with relatively high aggregate settling speeds is an expected characteristic of the natural and engineered environments of interest here.

3.2. Minimum separation gap representing the van der Waals interaction

In saline or brackish water body (for instance, marine systems or treatment systems with high ionic strength), the

electric double layer interaction [16,17] is suppressed, leaving the van der Waals attraction as the dominant interparticle interaction between colloidal particles. Several studies of aggregation simulation have used certain minimum gap criteria to represent irreversible attachment by the van der Waals attraction: a relatively small gap, 0.01% of a primary particle radius a, was used to calculate the collision efficiency between two nonporous settling spheres with different sizes [4,18]; and 0.1% of the radius was used to calculate random packing ratio by a certain simulation algorithm, called "sequential dropping and rolling" of spheres [19]. Doublet formation of spheres in differential settling was studied by Mazzolani et al. [6], using trajectory analysis between two interacting spheres via the van der Waals and hydrodynamic interactions with different size and density.

Hamaker calculated the van der Waals potential between two identical spheres [20] assuming the interaction instantaneously affects the spheres. However, the electric field, which is responsible for the London attraction between molecules, propagates with the speed of light between the particles. If a pair of molecules are widely separated, a time lag (or a phase difference) therefore develops between vibrations at the two locations [21]. The importance of this retardation increases as the separation distance becomes comparable to the wavelength of the propagating field. In this light, the Hamaker expression [20] becomes inaccurate when the gap between two non-Brownian particles is on the order of the particle size, since the electromagnetic retardation was assumed to be negligible while the pairwise additivity was applied. With the Derjaguin approximation, Schenkel and Ketchener [22] derived the retarded potential between two identical spheres, and Mazzolani et al. [6] used the corresponding retarded force as the negative gradient of the potential for the trajectory simulation.

Using a dimensionless retarded van der Waals force, defined in this study as

$$f = \frac{F_{\mathrm{RVDW}}}{6\pi\mu a V_0}, \tag{10}$$

where F_{RVDW} is the retarded van der Waals force as the negative derivative of Eq. (4) of Mazzolani et al.'s work, μ is the fluid viscosity, and V_0 is the fluid velocity that particles undergo, we performed simple numerical experiments to determine how well the minimum separation gap between two primary particles represents the retarded van der Waals force in calculations of particle–cluster aggregation. Fig. 1 shows the configuration of two equal-sized spherical particles of radius a: sphere 1 is held fixed at an origin of the coordinate system, and sphere 2 is approaching sphere 1 by uniform upward flow of a certain velocity V_0, being affected by the retarded van der Waals interaction. The free sinking velocity of an isolated sphere was chosen as the upward fluid velocity; i.e.,

$$V_0 = \frac{2a^2 g\Delta\rho}{9\mu}, \tag{11}$$

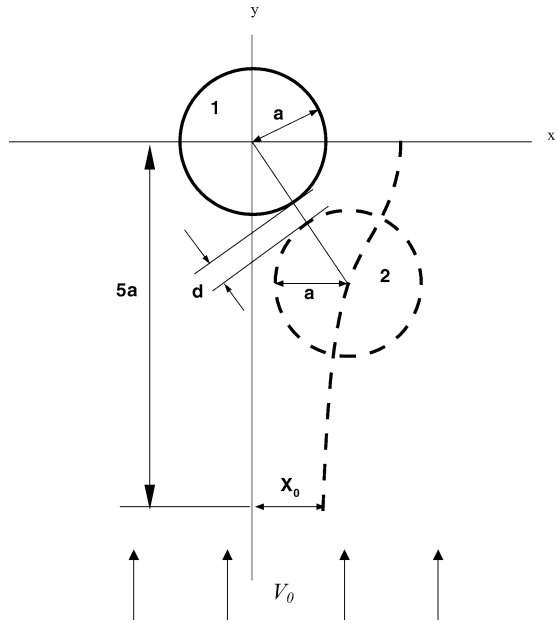

Fig. 1. Configuration of two spheres for analysis of the minimum separation gap that represents the effective force range of the retarded van der Waals attraction. Sphere 1 is held fixed at the origin of the coordinate, and sphere 2 is approaching sphere 1 from below, starting at $z = -5a$.

where $\Delta\rho = \rho_p - \rho_f$. Initially, sphere 2 is released at the point $(X_0, Y_0(= -5a))$, and continues to move upward with the fluid flow to the vicinity of sphere 1. A gap d between the two spheres is continuously measured until sphere 2 collides with sphere 1 or its center reaches the horizontal plane $(z = 0)$.

Fig. 2 shows the minimum separation gap d_{min} between the two spheres as a function of X_0, the distance to the center of sphere 2 from the vertical line passing through the center of sphere 1, with three different radii of 1, 5, and 10 μm for both spheres 1 and 2 (note: a sphere radius of 1 μm is used only for testing without Brownian effect). If sphere 2 was released at a point relatively far from the vertical line, i.e., $X_0/a \geqslant 2$, then d_{min} becomes a value on the order of the sphere radius a. The minimum separation gap d_{min}, however, rapidly converges to zero if X_0 decreases, particularly when it reaches a certain critical value, denoted by $X_{0,\mathrm{crit}}$. In other words, if sphere 2 starts at a distance X_0 less than the critical value $X_{0,\mathrm{crit}}$, it is essentially captured by sphere 1 due to the retarded van der Waals attraction. Results of the computer experiments shown in Fig. 3 represent the decrease of the critical point $X_{0,\mathrm{crit}}/a$ with increasing particle size. This is because the weighted force constant in Eq. (10) decreases with increasing particle size, resulting in weaker van der Waals attraction and more deviation of sphere 2 from sphere 1.

In this study, to reflect the particle size effect on the capturing force range, primary particle radii of 1.0, 0.1, and 0.01% are used as possible minimum separation gaps: if the surface-to-surface distance between two particles is less than the minimum separation gap, they are considered to be ag-

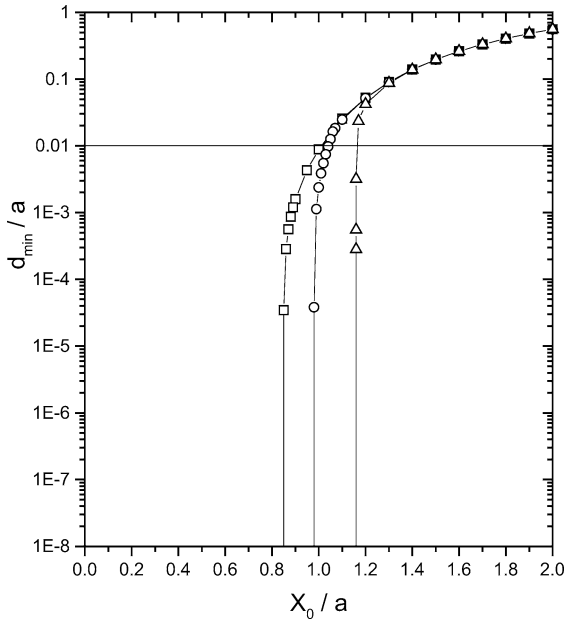

Fig. 2. Minimum separation gap between spheres 1 and 2 as a function of the distance between the center of sphere 2 and the vertical line passing through the center of sphere 1. Assumed parameter values are Hamaker constant $A_H = 4.113 \times 10^{-21}$ J and $\Delta\rho = 1.65$ g/cm^3 for $a = 1$ (△), 5 (○), and 10 μm (□).

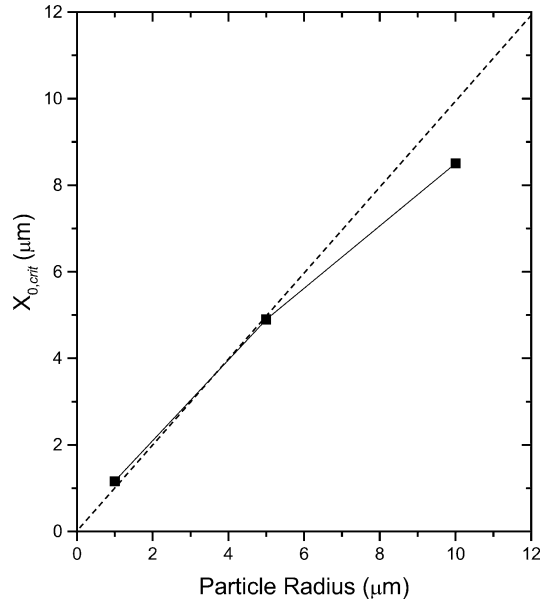

Fig. 3. Critical distance $X_{0,\mathrm{crit}}$ as a function of primary particle radius.

gregated to each other. The results of this sensitivity analysis are discussed in the following section.

3.3. Time interval

Determination of the proper time interval to avoid serious error propagation is considered as follows. The sinking velocity of the isolated sphere is obtained by balancing gravitational, buoyant, and Stokes drag forces; i.e.,

$$\frac{4\pi}{3}a^3(\rho_p - \rho_f)g = 6\pi\mu a V_0, \tag{12}$$

resulting in Eq. (11). A time scale for the movement of particles of radius a is then

$$T_{\mathrm{scale}} = \frac{a}{V_0} = \frac{9\mu}{2ag\Delta\rho}, \tag{13}$$

representing the necessary time to move the distance a (particle radius) with the velocity V_0. With this estimate, $0.01T_{\mathrm{scale}}$, considered small enough to avoid error propagation in the Runge–Kutta scheme, is chosen as the time interval Δt to perform simulations by solving the time evolution equation, Eq. (6).

3.4. Initial structure of the aggregate

When the simulation starts, the assumed configuration of an initial aggregate is a collection of seven identical spheres held together, of which the coordinates are $(\pm a, 0, 0)$, $(0, \pm a, 0)$, $(0, 0, \pm a)$, and $(0, 0, 0)$. This configuration is used to satisfy the fundamental assumption that the movement of the aggregate is not significantly affected by the presence of the single particle, due to the relatively large size and mass ratio. Therefore, even if the initial aggregate consists of only seven primary particles, it is expected that the assumed initial configuration is not strongly correlated with the structure of the final aggregate composed of 300 particles.

4. Collision efficiency

In this section, we present the method used to calculate global, capture, and collision efficiency of the generated aggregate.

4.1. Global efficiency η_{glo}

The primary spherical particle, denoted by g in Fig. 4, is released at the edge of the generated aggregate in the horizontal plane containing the center of mass of the aggregate, and then tracked backward in time until the limiting approach trajectory is found. The distance R_{glo} between the limiting trajectory and the vertical line passing through the center of mass is calculated 100 times; to average out the anisotropic structural effect of the aggregate, for each calculation of R_{glo} the aggregate is randomly rotated before a new primary particle is released at the edge of the aggregate. Details of this trajectory analysis method are described in the literature [4–6] for two impermeable spheres.

If the aggregate is considered as an (almost) impermeable sphere, this global efficiency converges to the collision efficiency between two solid particles with different sizes. In reality, however, aggregates are found to be porous and

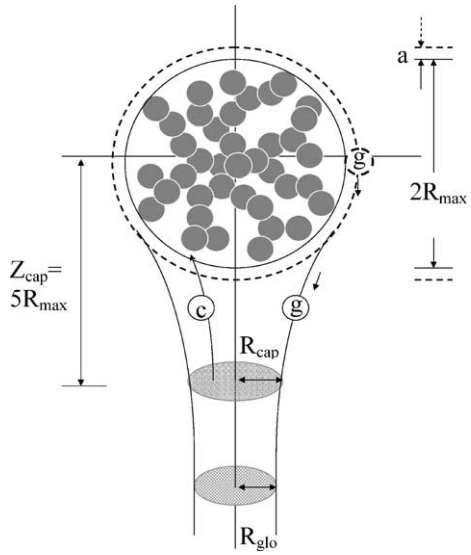

Fig. 4. Schematic plot of the coordinate system and the trajectories of sphere g and sphere c for the global and capture efficiencies, respectively.

permeable so that a single particle can penetrate and be captured by the aggregate. This effect is considered in the next section.

4.2. Capture efficiency η_{cap}

During the calculations of R_{glo} in the previous section, values of R_{cap}, a distance between the vertical line and the limiting trajectory at $z = -Z_{\text{cap}}$, are also recorded and averaged to determine the area in which a testing primary particle can start for the sake of capture efficiency estimation. To reduce the computational effort, the vertical distance between the circular area of which the radius is R_{cap} and the aggregate origin is set to five radii of the aggregate, i.e., $Z_{\text{cap}} = 5R_{\text{max}}$, since the limiting trajectory is found very far from the aggregate origin. The capture efficiency is defined as

$$\eta_{\text{cap}} = \frac{N_{\text{captured}}}{N_{\text{released}}}, \tag{14}$$

where N_{released} and N_{captured} are the number of primary particles released within the limiting trajectory at $z = -Z_{\text{cap}}$ and captured by the aggregate, respectively. A single particle (sphere c) is released 5000 times within the circular area of radius R_{cap}, and the captured number is counted to estimate the ratio of Eq. (14).

4.3. Aggregate collision efficiency E_{agg}

The (overall) collision efficiency of the aggregate, E_{agg}, is calculated by simple multiplication of the global and capture efficiencies; i.e.,

$$E_{\text{agg}} = \eta_{\text{glo}}\eta_{\text{cap}}, \tag{15}$$

representing the ratio of the number of particles released sufficiently far from and approaching the aggregate within a circle of radius $R_{\text{max}} + a$ to the number of particles captured within the interior of the aggregate.

5. Results and discussion

5.1. Aggregate structure and fractal dimension

The SD-based formalism, specially developed for particle–cluster aggregation, was used with the partitioning method [12] to decompose the grand mobility matrix, and two predetermined parameters (i.e., the time interval and the minimum separation gap) were appropriately selected for efficient calculation with the assumed initial structure of the aggregate. Without Brownian motion, a sufficiently small time-interval was determined to reduce possible error propagation, and the initial structure was assumed not to affect the structure of the fully grown aggregate composed of many primary particles. Fig. 5 shows three simulated aggregates of 300 primary particles, which formed in the differential settling process. Three different minimum separation gaps, $0.01a$, $0.001a$, and $0.0001a$, were used to examine sensitivity of aggregate structure. The three aggregates commonly have globally spherical, but locally anisotropic, clumped structure with similar length scales represented by R_{max}: the aggregates generated have $R_{\text{max}} = 23.55a$ with the gap of $0.01a$, $R_{\text{max}} = 22.96a$ with $0.001a$, and $R_{\text{max}} = 23.66a$ with $0.0001a$, showing structural indifference to the minimum separation gap.

The aggregate structures were characterized by fractal dimensions, which were calculated by the slope of $\log(r/a)$ vs $\log(N)$ plot as shown in Fig. 6, being assumed to follow the power law in [23]; i.e.,

$$N(r) \propto \left(\frac{r}{a}\right)^{D}, \tag{16}$$

where $N(r)$ is the number of primary particles within the radial distance $r \leqslant R_{\text{max}} + a$, and D is the fractal dimension of the aggregate. The three aggregates illustrated in Fig. 5 have similar number profiles of primary particles as shown in Fig. 6, and the corresponding fractal dimensions are $D = 1.99$ with $d_{\text{min}}/a = 0.01$, $D = 1.98$ with $d_{\text{min}}/a = 0.001$, and $D = 2.00$ with $d_{\text{min}}/a = 0.0001$. The averaged fractal dimension of 1.99 is almost identical to the fractal dimension of 1.98 [24] that was obtained from a two-point density–density correlation function [25] with a similar aggregate generated by the same algorithm.

The particle–cluster aggregation formalism used in this study for differential settling yields the common fractal dimension of $D \simeq 2.0$, which can be compared to fractal dimensions of aggregates generated by other mechanisms: diffusion-limited aggregation (DLA), diffusion-limited cluster aggregation (DLCA), and reaction-limited cluster aggregation (RLCA).

In the DLA model, primary particles are added, one at a time, to a growing cluster via random walk trajectories start-

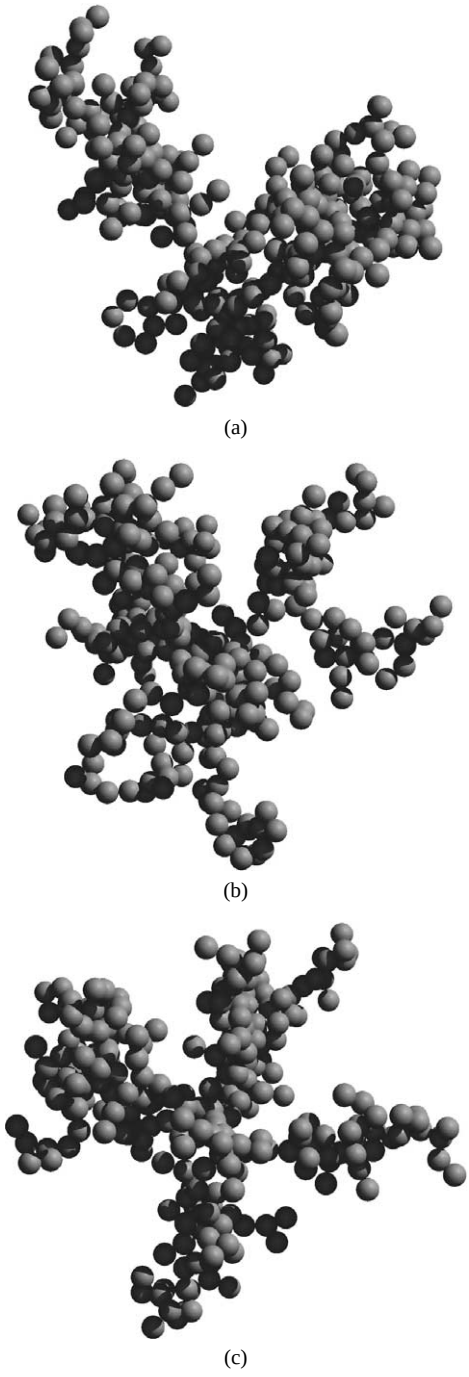

Fig. 5. Aggregates of 300 particles generated by differential settling with $d_{\min}/a =$ (a) 0.01, (b) 0.001, and (c) 0.0001 and $R_{\max} = 23.55a$, $22.96a$, and $23.66a$, respectively.

ing from outside of the region occupied by the growing cluster. This model generates random clusters that can be characterized by fractal dimensions of $D = 1.68$–1.70 [26–28] in two-dimensional space. Bensimon et al. [29] also had generated an aggregate in the two-dimensional space, considering the "sticking length" and the "mean free path" of the diffusing particles. In their method, seed particles were moving on radial straight lines from outside of the growing aggregate with uniformly distributed orientation, providing a fractal dimension of $D = 1.93$ slightly greater than ~ 1.7 [26–28]. In three-dimensional space, Meakin found that the DLA mechanism gives us a fractal dimension of $D \sim 2.5$ [27], which is remarkably higher than that in two-dimensional case, showing that the fractal dimensions are significantly affected by the Euclidean dimension in which the aggregates are created.

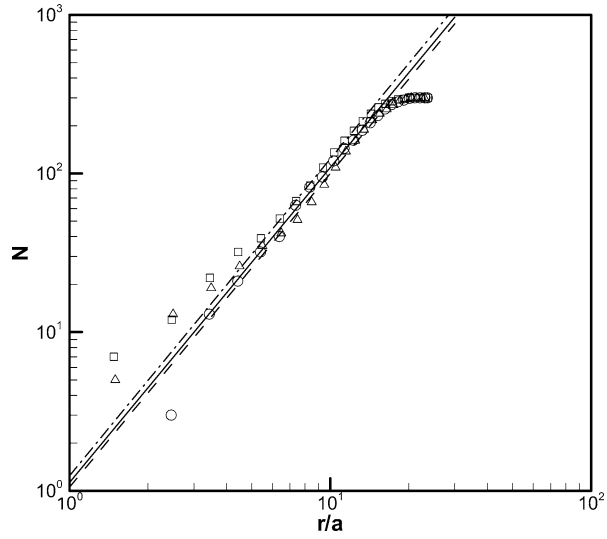

Fig. 6. Accumulated number profile of primary particles, N, as a function of dimensionless radius r/a for three aggregates formed in differential settling with different minimum separation gaps. The slope of the each line represents the fractal dimension of the individual aggregate: $D = 1.99$ (solid) with $d_{\min}/a = 0.01$ (○), $D = 1.98$ (dashed) with $d_{\min}/a = 0.001$ (△), and $D = 2.00$ (dash–dotted) with $d_{\min}/a = 0.0001$ (□).

In the DLCA model, clusters are not formed by the sequential addition of particles to a growing cluster as aggregate: instead, aggregation phenomenon occurs throughout the system. Initially, pairs of particles join to form binary clusters (i.e., dimmers) that continue to move and join with other particles or clusters to form larger and larger structures. The process of cluster growth with the DLCA mechanism was investigated by a Monte Carlo method [30], providing a fractal dimension of $D = 1.38$ in the Euclidean dimension of $d = 2$. Similar simulations with relatively larger numbers of particles, compared to Kolb et al.'s work [30], were performed by Meakin [31], and a slightly higher fractal dimension of $D \sim 1.50$ was provided. Weitz and Olivera [32] used transmission-electron microscope (TEM) to investigate the structure formed by the irreversible kinetic aggregation of equal-sized gold colloids; $D = 1.75$ was found by their experiments, and is considered as the typical fractal dimension of the DLCA mechanism in the Euclidean dimension of $d = 3$.

Relatively less research has been done in the RLA compared to the RLCA. The chance of sticking as a result of a collision event is assumed to be very small in the RLCA mechanism, which allows colliding clusters to bounce off one another and explore all possible aggregation conformations, providing denser structures with fractal dimensions of $D \sim 1.51$–1.56 [33] in $d = 2$ and $D \sim 1.90$–2.06

in $d = 3$ [33–35]. These studies used a hierarchical lattice model in which 2^n particles are first combined to form 2^{n-1} binary clusters, and then the binary clusters are combined to 2^{n-2} clusters, each containing four lattice sites, leaving only one cluster after n consecutive stages. Meakin and Family [36,37] developed three models of the RLCA mechanism, providing $D = 1.61$ and 2.09 in two- and three-dimensional space, respectively [38]. Most of the RLCA models described above, however, are lattice-based models except one with random rotation in an off-lattice [36,37].

Structures of fractal colloidal aggregates formed in both DLCA and RLCA (and the crossover region) were studied by static light-scattering experiments [39], and were found to have fractal dimensions of $D = 1.86$ for the DLCA and 2.13 for the RLCA. Moreover, other experimental investigations with settling aggregates showed fractal dimensions of $D \sim$ 1.8–2.3 controlled by interparticle interactions [3,40].

Three-dimensional Monte Carlo simulations were recently performed to study the sol–gel transition in the DLCA process [41,42], and it was found that in the flocculation regime, in which several aggregates are formed and are still growing, the aggregate has a fractal dimension of $D = 1.8$, and in the percolation regime, in which only one big aggregate remains, the aggregate has a fractal dimension of $D = 2.5$, in good agreement with Meakin's DLA work [27]. These results indicate that the DLA in two-dimensional space and the DLCA in three dimensions have similar fractal dimension values of $D \sim 1.7$–1.8, and the final aggregates, left in the DLA with $d = 3$ as well as in the percolation regime of the DLCA, have the common fractal dimension of $D = 2.5$.

Our simulation is similar to the RLA mechanism in three-dimensional Euclidian space since non-Brownian particles are considered only with hydrodynamic interactions which are, in general, long-ranged and repulsive. This similarity is also verified by the fractal dimension of $D \simeq 2.0$ of our work since it is close to 2.1, which is the typical fractal dimension value of the three-dimensional RCLA mechanism. Without considering breakage or reworking of aggregates during differential settling in stationary flow, it is likely that sole particle–cluster aggregation with repulsive interaction results in a similar fractal dimension of cluster–cluster aggregation with the same repulsive interaction. The possible reason is that collision opportunity between two different (especially small) aggregates is also rare in the RLCA like the opportunity between the primary particle and the aggregate in our differential settling simulations. In this light, the effect of a deterministic trajectory without random Brownian movement is considered to be important, as observed in fractal dimensions of the DLA produced by random walk ($D \sim 1.7$) [26–28] and by straight trajectory simulation ($D \sim 1.9$) [29].

In addition, the minimum separation distance $d_{\min}$ represents the force range of the retarded van der Waals attraction as an origin of irreversible sticking. When $d_{\min}$ is added to the particle diameter $2a$, $2a + d_{\min}$ corresponds to the sticking length scale l_s of Bensimon et al.'s work [29]. As shown in Fig. 6 and Table 1, the fractal dimension of the generated aggregate is completely indifferent to the minimum separation distance, implying that the effect of particle size on the fractal dimension is negligible for non-Brownian particles. Another important length scale is the displacement of the primary particle in each time step, which was called the "mean free path l_0 of diffusing particles" [29]. In our case, however, the mean free path is controlled by the sufficiently small time interval Δt so that the ratio of the displacement to the particle radius a is an order of $O(10^{-2})$. Therefore, it is also believed that, similar to the insensitiveness of the fractal dimension to the minimum separation gap, any smaller value of the time interval does not remarkably affect the common fractal dimension of the aggregates obtained in this study.

Table 1
Sensitivity analysis of fractal dimensions, and global, capture, and collision efficiencies of the three generated aggregates with variation of the minimum separation gap $d_{\min}$

$d_{\min}/a$	D_f	$\eta_{\text{glo}} \times 10^1$	$\eta_{\text{cap}} \times 10^2$	$E_{\text{agg}} \times 10^3$
10^{-2}	1.99	2.03	3.20	6.49
10^{-3}	1.98	1.61	3.12	5.02
10^{-4}	2.00	1.96	2.96	5.79
Average	1.99 ± 0.01	1.87 ± 0.22	3.09 ± 0.12	5.77 ± 0.73

5.2. *Efficiency and structure of the generated aggregate*

The collision efficiencies obtained as the product of the global and the capture efficiencies are given in Table 1 for each assumed minimum separation distance. The calculated efficiencies vary about 10–20% in a nonmonotonic manner as the minimum separation distance is reduced. This variation may be due in part to the stochastic nature of the simulations, but in any case is sufficiently small to validate the minimum separation distance as a way of representing the interparticle forces. Because the minimum separation gap can be thought of as related to the attachment efficiency of collisions, the question arises as to why there is not more sensitivity of the aggregate structure and the efficiencies to the value of the minimum separation gap. However, this lack of sensitivity is consistent with the results shown in Fig. 2 for collisions of two spheres. For each size of particle represented in these calculations (between 1 and 10 μm), the "attachment efficiency" represented by the value of $X_{0,\text{crit}}/a$ is almost the same for the entire range of relative minimum separation gaps between 10^{-4} and 10^{-2}. Changes in "attachment efficiency" would be expected only for larger values of assumed minimum separation distances. The average of the global efficiencies, calculated using the average of $R_{\text{glo}}^2/R_{\max}^2$ rather than the square of $\langle R_{\text{glo}}/R_{\max}\rangle$ is $1.87(\pm 0.22) \times 10^{-1}$. The average capturing efficiency is found to be $3.09(\pm 0.12) \times 10^{-2}$. These two averaged (global and capturing) efficiencies lead to the final collision efficiency of $E_{\text{agg}} = 5.77(\pm 0.73) \times 10^{-3}$, which is almost iden-

tical to an average of three E_{agg} values for three different minimum separation gaps in Table 1.

The collision efficiency of $5.77(\pm 0.73) \times 10^{-3}$ calculated by this study can be compared to values of other previous studies. For a size ratio of $a/R_{max} = 1/20$, which is close to the value of $\sim 1/23$ in this study (see Fig. 5), Han and Lawler [4] calculated collision efficiencies between two impermeable spheres, and the values were on the order of 10^{-3}–10^{-2} with the Hamaker constant A_H ranging from $2k_BT$ to $50k_BT$. Although the collision efficiency value for $A_H = 10k_BT$ was about 5×10^{-3}, which is close to our calculation, the same mass density was commonly used for both large and small impermeable spheres in their work.

Mazzolani et al. [6] clearly showed that when the small particle is denser than the large one, as is the case for this study, the collision efficiency can be significantly reduced in comparison to the equal density case. To compare Mazzolani et al.'s work to the current work, it is assumed that the primary particles have radius $a = 10$ μm and specific gravity 2, leaving a reduced density ratio, defined by Mazzolani et al., of $\gamma = 40.55$. With Eq. (19) of their work, which is the asymptotic limit derived for $\gamma \gg 1$, an efficiency of about 8.0×10^{-11} is obtained with $A_H = k_BT$. The correct theoretical value of the efficiency with $\gamma = 40.55$ and $a/R_{max} = 1/23$ may be smaller than 8.0×10^{-11} because they did not make complete calculations for this range of γ and a/R_{max}.

Stolzenbach [43] calculated the scavenging efficiency of a settling porous sphere, assuming that small particles follow the flow field toward the porous sphere without experiencing any interparticle interaction, and that sticking of small particles within the permeable sphere is relatively efficient. Using the parameters of our study, Stolzenbach's assumptions lead to a global efficiency of 0.109 and a capture efficiency of 0.573. This theoretical global efficiency value for the uniformly permeable sphere is close to our value of ~ 0.187 for the fractal aggregates generated by the SD-based simulation. The reason two approaches provide similar values of the global efficiency is self-explanatory: during the simulation, to avoid anisotropic structural effect of the generated aggregates to the averaged global efficiency, the aggregates are randomly rotated for each of 100 backward trajectory simulations. The global efficiency obtained in our study, 0.187, therefore reflects a mean isotropic property of the fractal aggregate, indicating that the effect of overall porosity (or permeability) is more important to the global efficiency compared to the local structure of the aggregate. The difference between the global efficiencies of the simulation and the theory is due to the combination of clumped and (almost) void outer regions within the aggregate shown in Fig. 5 (unlike the completely smooth surface of the uniformly porous sphere), in which flow field is less or more deflected.

The capture efficiency of our study, 0.0309, is one order of magnitude smaller than that of Stolzenbach's theory, indicating that the assumptions made by Stolzenbach with regard to capture of small particles greatly overestimate the actual capture probability. As shown in Fig. 5, the created aggregates generally have an almost spherical (in outer shape), but anisotropic structure with a fluctuating number (or mass) density along the azimuthal direction, so that a high proportion of the intercepted flow can pass through the outer portion of the fractal aggregate, in which attached particles are sparsely populated, leading to the low capture rates. In other words, unlike the case of the uniformly porous sphere, the fluid flow preferentially penetrates the aggregate through void space between locally clumped regions. Nevertheless, only the local dense region contributes to the capture efficiency, causing the difference between two approaches explained above, while the global efficiency is mainly affected by mean field of the locally dense and sparse regions.

6. Concluding remarks

A new method of application of Stokesian dynamics simulation for generating a fractal aggregate and predicting collision efficiency between the sinking fractal aggregate and a suspended primary particle in differential settling process was presented. The attractive van der Waals force causing irreversible sticking of the primary particle to the fractal aggregate was represented by an assumed minimum separation gap. However, structural indifference of aggregates was found by common fractal dimension values obtained with different minimum separation gaps, indicating that the effect of primary particle size on the fractal dimension is negligible for non-Brownian particles. The averaged global and capture efficiencies were $1.87(\pm 0.22) \times 10^{-1}$ and $3.09(\pm 0.12) \times 10^{-2}$, respectively, providing a collision efficiency of $5.77(\pm 0.73) \times 10^{-3}$. This result was somewhat (10–20%) sensitive to the minimum separation gap. Compared to a uniformly porous sphere, a fractal aggregate of the same size with clumped local structure provided the similar global efficiency, but the capture efficiency of the fractal aggregate was one order of magnitude lower than that of the uniformly porous sphere. These findings lead to the conclusion that, although the global collision efficiency of permeable aggregates may be higher than that of impermeable spheres of the same size by orders of magnitude, the potential large increase in collision efficiency resulting from small particles moving with the flow into a sinking aggregate is partially offset by the low capture efficiency associated the outer sparse portion of a fractal aggregate. Although the calculation of particle capture efficiency, even done efficiently, is computationally expensive, additional simulations would shed light on the inherent stochastic variability of the results as well as sensitivity to assumed parameters.

References

[1] M. Elimelech, J. Gregory, X. Jia, W. Williams, Particle Deposition and Aggregation: Measurement, Modeling, and Simulation, Butterworth Heinemann, Oxford, 1995.

[2] X. Li, B.E. Logan, Environ. Sci. Technol. 31 (1997) 1237.
[3] X. Li, B.E. Logan, Environ. Sci. Technol. 31 (1997) 1229.
[4] M. Han, D.F. Lawler, J. Hydraul. Eng. 117 (1991) 1269.
[5] E. Wacholder, N.F. Sather, J. Fluid Mech. 65 (1974) 417.
[6] G. Mazzolani, K.D. Stolzenbach, M. Elimelech, J. Colloid Interface Sci. 197 (1998) 334.
[7] J.F. Brady, G. Bossis, Annu. Rev. Fluid Mech. 20 (1988) 111.
[8] D.J. Jeffrey, Y. Onishi, J. Fluid Mech. 139 (1984) 261.
[9] S. Kim, R.T. Mifflin, Phys. Fluids 28 (1985) 2033.
[10] L. Durlofsky, J.F. Brady, G. Bossis, J. Fluid Mech. 180 (1987) 21.
[11] G. Bossis, A. Meunier, J.F. Brady, J. Chem. Phys. 94 (1991) 5064.
[12] V.N. Faddeeva, Computational Methods of Linear Algebra, Dover, New York, 1959.
[13] S. Kim, Dynamics of Particle Accumulation at Engineered and Natural Interfaces, Ph.D. thesis, University of California, Los Angeles, 2000.
[14] W.H. Press, S.A. Teukosky, W.T. Vetterling, B.P. Flannery, Numerical Recipes in FORTRAN, Cambridge Univ. Press, New York, 1992.
[15] G.K. Batchelor, J. Fluid Mech. 98 (1980) 609.
[16] B.V. Derjaguin, L.D. Landau, Acta Physicochim. URSS 14 (1941) 733.
[17] E.J. Verwey, J.T.G. Overbeek, Theory of the Stability of Lyophobic Colloids, Elsevier, Amsterdam, 1948.
[18] M. Han, Mathematical Modeling of Heterogeneous Flocculent Sedimentation, Ph.D. thesis, University of Texas at Austin, 1989.
[19] G.T. Nolan, P.E. Kavanagh, Powder Technol. 72 (1992) 149.
[20] H.C. Hamaker, Physica 4 (1937) 1058.
[21] P.C. Hiemenz, Principles of Colloid and Surface Chemistry, Dekker, New York, 1986.
[22] J.H. Schenkel, J.A. Kitchener, Trans. Faraday Soc. 56 (1960) 161.
[23] S. Veerapaneni, M.R. Wiesner, J. Colloid Interface Sci. 177 (1996) 45.
[24] A.S. Kim, K.D. Stolzenbach, J. Colloid Interface Sci. 253 (2002) 315, doi:10.1006/jcis.2002.8525.
[25] P. Meakin, Rev. Geophys. 29 (1991) 317.
[26] P. Meakin, Phys. Rev. A 27 (1983) 604.
[27] P. Meakin, Phys. Rev. A 27 (1983) 1495.
[28] T.A. Witten, L.M. Sander, Phys. Rev. Lett. 47 (1981) 1400.
[29] D. Bensimon, E. Domany, A. Aharony, Phys. Rev. Lett. 51 (1983) 1394.
[30] M. Kolb, R. Botet, R. Jullien, Phys. Rev. Lett. 51 (1983) 1123.
[31] P. Meakin, Phys. Rev. Lett. 51 (1983) 1119.
[32] D.A. Weitz, M. Olivera, Phys. Rev. Lett. 52 (1984) 1433.
[33] R. Jullien, J. Phys. A 17 (1984) L771.
[34] R. Jullien, M. Kolb, J. Phys. A 17 (1984) L639.
[35] M. Kolb, R. Jullien, J. Phys. France Lett. 45 (1984) L977.
[36] P. Meakin, F. Family, Phys. Rev. A 38 (1988) 2110.
[37] P. Meakin, F. Family, Phys. Rev. A 36 (1987) 5498.
[38] P. Meakin, Ann. Rev. Phys. Chem. 39 (1988) 237.
[39] M.Y. Lin, R. Klein, H.M. Lindsay, D.A. Weitz, R.C. Ball, P. Meakin, J. Colloid Interface Sci. 137 (1990) 263.
[40] C.P. Johnson, X. Li, B.E. Logan, Environ. Sci. Technol. 30 (1996) 1911.
[41] J.C. Gimel, D. Durand, T. Nicolai, Phys. Rev. B 51 (1995) 11,348.
[42] J.C. Gimel, T. Nicolai, D. Durand, J. Sol–Gel Sci. Technol. 15 (1999) 129.
[43] K.D. Stolzenbach, Deep-Sea Res. 40 (1993) 359.